

Electronic Supplementary Information for

Cobalt-doping in Cu_2SnS_3 : Enhanced thermoelectric performance by synergy of phase transformation and band structure modification

Huiwen Zhao^a Xiaoxuan Xu^a Chao Li^b Ruizhi Zhang^c Rong Huang^b Yinong Lv^a Dongxu Li^a Xiaohui Hu^a Lin Pan^{*a} and Yifeng Wang^{*a}

Supplemental Note 1: Calculations of effective masses and Lorenz numbers

From the single parabolic band model (SPB) where acoustic phonon scattering as the main carrier scattering mechanism ($s = 0$), Seebeck coefficient and carrier effective mass (m^*) were calculated from the following equations¹:

$$S = \frac{k_B}{e} \left[\frac{(s+2)F_1(\eta)}{(s+1)F_0(\eta)} - \eta \right] \quad (1)$$

$$m^* = \frac{\hbar^2}{2k_B T} \left[\frac{n_e}{4\pi F_1(\eta)} \right]^{2/3} \quad (2)$$

where $F_s(\eta)$ is the Fermi integral defined as:

$$F_n(\eta) = \int_0^\infty \frac{x^n}{1 + e^{x-\eta}} dx \quad (3)$$

Where k_B is Boltzmann's constant, e is electron charge, s is scattering parameter, η is the reduced chemical potential, and \hbar is Planck constant.

$$L = \left(\frac{k_B}{e} \right)^2 \frac{3F_0(\eta)F_2(\eta) - 4F_1(\eta)^2}{F_0(\eta)^2} \quad (4)$$

Supplemental Note 2: Calculations of average sound speed, Grüneisen parameters(γ), Young's modulus (E), shear modulus (G) and bulk modulus(K).

Average velocity v_{avg} can be extracted from:

$$v_{avg} = \left[1/3 \left(\frac{1}{v_L^3} + \frac{2}{v_T^3} \right) \right]^{-1/3} \quad (5)$$

Here, the longitudinal (v_L) and transverse (v_T) sound velocities have been obtained as described in the experimental details section.

The Grüneisen parameter can be calculated by:^{2,3}

$$\gamma = \frac{3}{2} \left(\frac{1 + \nu_p}{2 - 3\nu_p} \right) \quad (6)$$

where Poisson ratio ν_p can be derived from the v_L and v_T by:

$$\nu_p = \frac{1 - 2(v_T/v_L)^2}{2 - 2(v_T/v_L)^2} \quad (7)$$

Young's modulus (E) can be derived from the v_L and v_T by the relationship as:⁴

$$E = \frac{\rho(3v_L^2 - 4v_T^2)}{3} \quad (8)$$

Shear modulus (G) and bulk modulus(K) can be calculated by:

$$G = \frac{E}{2(1 + \mu)} \quad (9)$$

$$K = \frac{E}{3(1 - 2\mu)} \quad (10)$$

Supplemental Figures and Tables

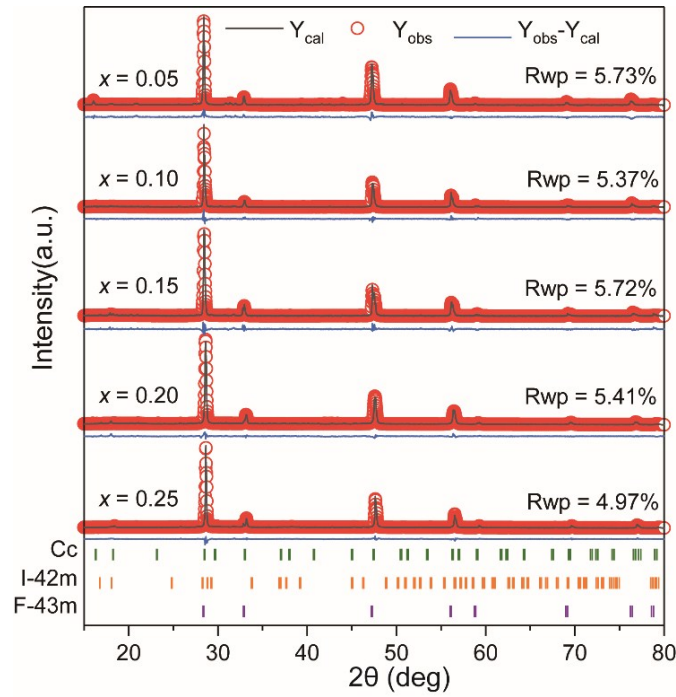


Fig. S1 Rietveld refinement results for $\text{Cu}_2\text{Sn}_{1-x}\text{Co}_x\text{S}_3$ samples with $x = 0.05-0.25$ using Profex program, which deduce the mole ratio of the monoclinic, cubic and tetragonal phases.

Table S1. Crystal structure parameters of $\text{Cu}_2\text{Sn}_{1-x}\text{Co}_x\text{S}_3$ ($x = 0.05-0.25$) obtained from refinement of XRD.

x	Mole mass ratio	Lattice parameter(\AA)			R_{wp} (%)
		a	b	c	
0.05	Cc (46.15%)	6.644	11.563	6.654	6.73
	F-43m (45.76%)	5.436	5.436	5.436	
	I-42m (8.09%)	5.434	5.434	10.716	
0.10	Cc (21.26%)	6.701	11.553	6.631	6.37
	F-43m (54.57%)	5.430	5.430	5.430	

	I-42m (24.17%)	5.409	5.409	10.857	
	Cc (7.68%)	6.720	11.453	6.606	
0.15	F-43m (60.51%)	5.420	5.420	5.420	6.72
	I-42m (31.81%)	5.398	5.398	10.896	
	Cc (4.98%)	6.704	11.441	6.598	
0.20	F-43m (36.65%)	5.411	5.411	5.411	5.41
	I-42m (58.37%)	5.402	5.402	10.825	
	Cc (2.57%)	6.586	11.505	6.630	
0.25	F-43m (28.06%)	5.401	5.401	5.401	4.97
	I-42m (69.37%)	5.399	5.399	10.793	

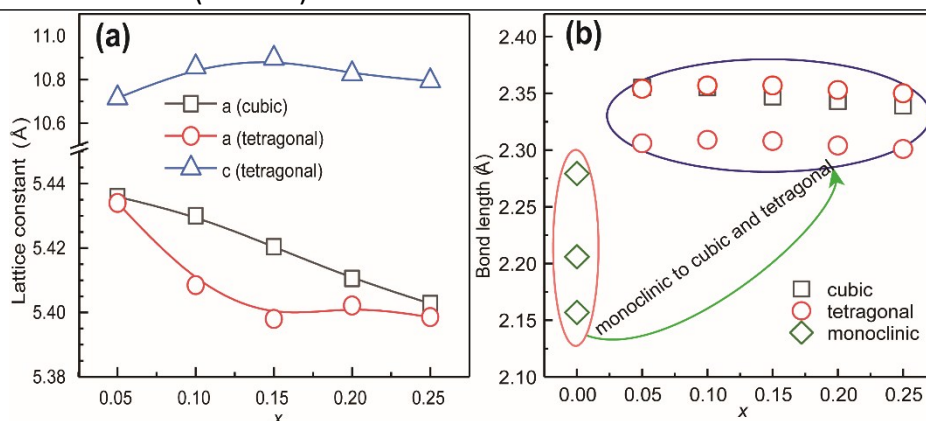


Fig. S2 Comparison of (a) the lattice constants a and c , and (b) the M-S bond lengths in the cubic, tetragonal phases with those short in the monoclinic phase co-existing in $\text{Cu}_2\text{Sn}_{1-x}\text{Co}_x\text{S}_3$ ($x = 0.05-0.25$) from the refinement results of XRD.

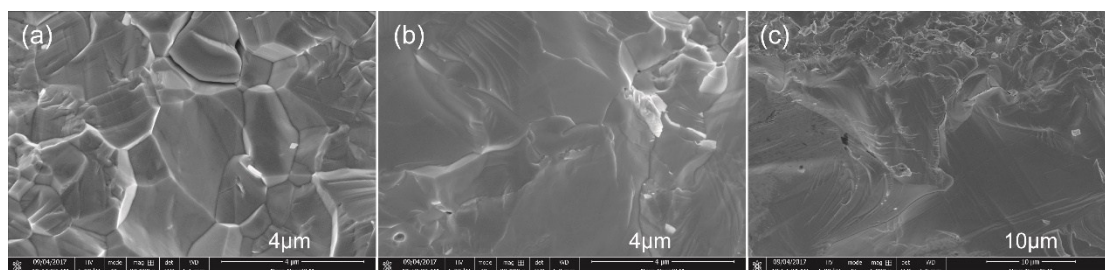


Fig. S3 SEM images of the fractured surface of $\text{Cu}_2\text{Sn}_{1-x}\text{Co}_x\text{S}_3$ (a) $x = 0$ (b) $x = 0.15$, (c) $x = 0.20$. The grain size of $\text{Cu}_2\text{Sn}_{1-x}\text{Co}_x\text{S}_3$ samples is uneven ranging from several microns to dozens of microns.

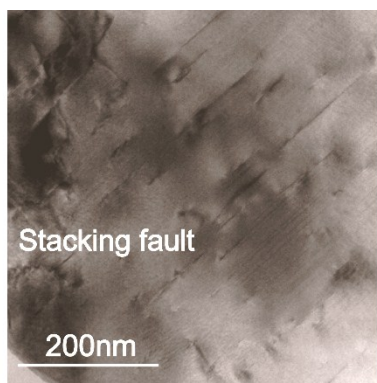


Fig. S4 The stacking fault with a size of 100-200 nm can be seen in $\text{Cu}_2\text{Sn}_{1-x}\text{Co}_x\text{S}_3$ ($x = 0.05$).

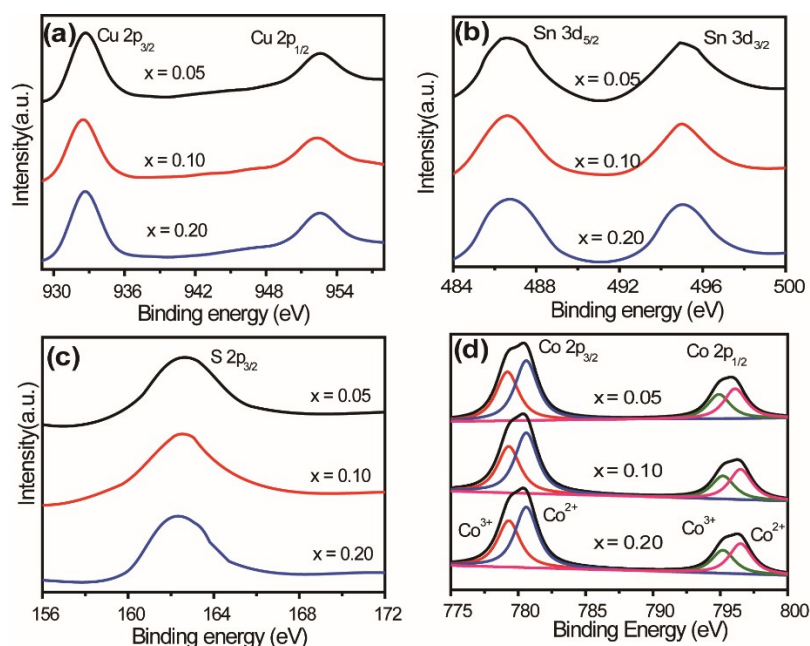


Fig. S5 XPS analysis of $\text{Cu}_2\text{Sn}_{1-x}\text{Co}_x\text{S}_3$ ($x = 0.05, 0.10, 0.20$) bulk samples: (a) Cu 2p; (b) Sn 3d; (c) S 2p; (d) Co 2p.

To confirm the oxidation state of the metal cations, XPS analysis (Fig. S4) was conducted. It displays the high-resolution XPS profiles of the four elements: Cu 2p, Sn 3d, S 2p and Co 2p of $\text{Cu}_2\text{Sn}_{1-x}\text{Co}_x\text{S}_3$ ($x = 0.05, 0.10, 0.20$). They change little with the increase of doping amount. The peak of Cu $2p_{3/2}$ and Cu $2p_{1/2}$ with binding energy 932.5 and 952.3 eV which agrees with Cu^+ (a peak separation of 19.8 eV) in Fig. S4(a). Fig. S4(b) shows Sn $3d_{5/2}$ and Sn $3d_{3/2}$ peaks locate at 486.3 and 494.7 eV agrees with Sn^{4+} (a peak separation of 8.4 eV). Fig. S4(c) shows the S 2p peaks locating at 163.0 eV corresponding to S^{2-} state. Fig. S4(d) shows the binding energy of the corresponding Co $2p_{3/2}$ and Co $2p_{1/2}$ core levels of 780.6 and 796.5 eV accords with Co^{2+} , respectively. A strong shake-up satellite structure at 779.3 and 795.2 eV can be seen obviously. In order to determine if the spectra contained other valence states Co, we fitted them considering an additional doublet at the binding energy. Finely, Co^{3+} has been found to conform to the separated peak with the binding energy of 779.3 and 795.2 eV⁵ which demonstrate Co^{2+} and Co^{3+} coexist in $\text{Cu}_2\text{Sn}_{1-x}\text{Co}_x\text{S}_3$. The existence of Co^{3+} makes the structure transition and electrical transport properties more complex.

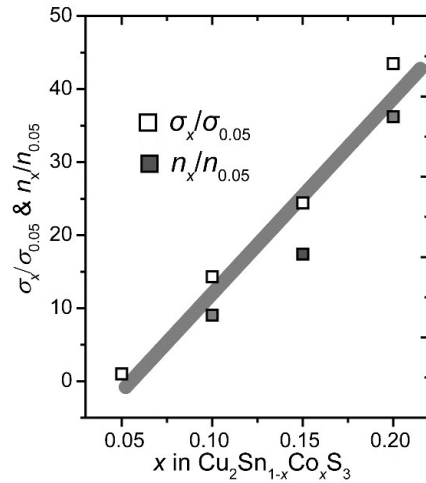


Fig. S6 The ratio of σ and n with samples $\text{Cu}_2\text{Sn}_{1-x}\text{Co}_x\text{S}_3$ ($x = 0.05-0.20$ to the $x = 0.05$) at 323K.

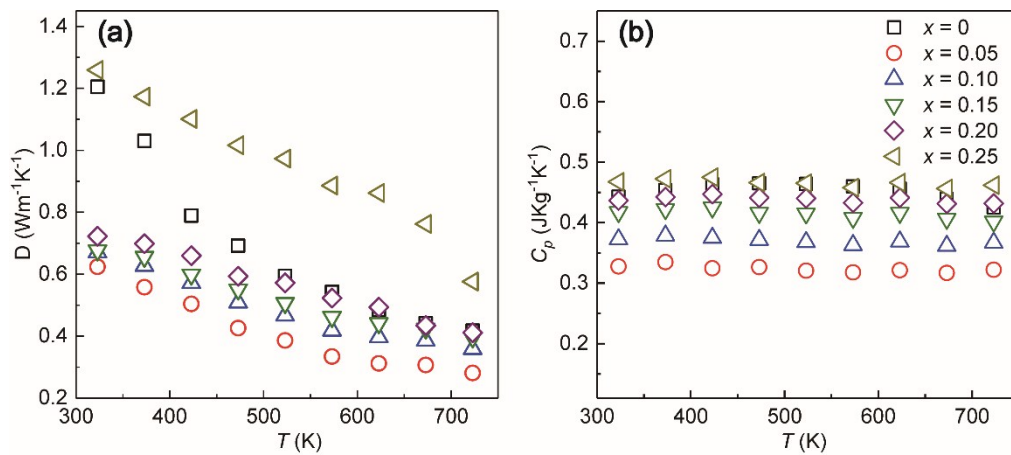


Fig. S7 The thermal diffusivity (a) and specific heat data (b) of $\text{Cu}_2\text{Sn}_{1-x}\text{Co}_x\text{S}_3$ ($x = 0-0.25$).

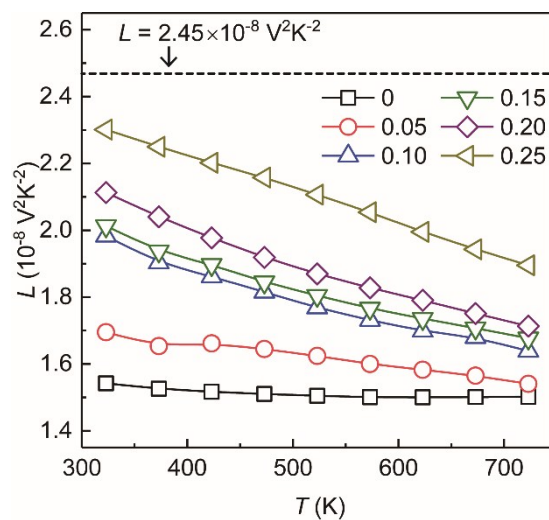


Fig. S8 The calculated temperature-dependent Lorenz number of $\text{Cu}_2\text{Sn}_{1-x}\text{Co}_x\text{S}_3$ samples with $x = 0-0.25$.

References

1. C. B. Vining, *J. Appl. Phys.*, 1991, 69, 331-341.
2. L.-D. Zhao, J. He, D. Berardan, Y. Lin, J.-F. Li, C.-W. Nan and N. Dragoe, *Energy Environ. Sci.*, 2014, 7, 2900.
3. F. Bocher, S. P. Culver, J. Peilstocker, K. S. Weldert and W. G. Zeier, *Dalton tran.*, 2017, 46, 3906-3914.
4. P. Ying, X. Li, Y. Wang, J. Yang, C. Fu, W. Zhang, X. Zhao and T. Zhu, *Adv. Funct. Mater.*, 2017, 27, 1604145.
5. G. Fierro, M. L. Jacono, M. Inversi, R. Dragone and P. Porta, *Top. Catal.*, 2000, 10, 39-48.